



## CONTRIBUTION OF GLACIER, SNOW AND RAIN COMPONENTS IN FLOW REGIME PROJECTED WITH HBV UNDER AR5 BASED CLIMATE CHANGE SCENARIOS OVER CHITRAL RIVER BASIN (*HINDUKUSH RANGES, PAKISTAN*)

Burhan A.<sup>1+</sup>

M. Usman<sup>2</sup>

S. A. A. Bukhari<sup>3</sup>

H. Sajjad<sup>4</sup>

<sup>1,2,3,4</sup>Research and Development Division, Pakistan Meteorological Department, Islamabad, Pakistan.

<sup>1</sup>Email: [burhanahmadkhan@gmail.com](mailto:burhanahmadkhan@gmail.com) Tel: +92-51-9250361

<sup>2</sup>Email: [usman666.m@gmail.com](mailto:usman666.m@gmail.com) Tel: +92-51-9250361

<sup>3</sup>Email: [ahsanpmd@gmail.com](mailto:ahsanpmd@gmail.com) Tel: +92-51-9250361

<sup>4</sup>Email: [sajjadhaider76@yahoo.com](mailto:sajjadhaider76@yahoo.com) Tel: +92-51-9250361



(+ Corresponding author)

### ABSTRACT

#### Article History

Received: 18 March 2020

Revised: 20 April 2020

Accepted: 22 May 2020

Published: 16 June 2020

#### Keywords

HBV

Hydrological modeling

Climate Change

Chitral River Basin

Snowmelt

Glacier-melt.

Knowledge of projection and attribution of streamflow composition in rain and snow fed glaciated catchments has been of vital significance to a spectrum of stakeholder communities. Accordingly, assessment of contributed share of rain, snow and glacier to downstream flow regime in snowy and glaciated catchment area of Chitral River Basin (CRB) in historical and projected periods was made in this study. HBV-Light hydrological model (hereafter HBV) was used to identify temporal variation and composition of streamflow in response to alterations in hydro-meteorological parameters over the CRB. The HBV was seen to perform fairly well both during calibration ( $R^2=0.91$ ,  $Reff=0.91$ ) and validation ( $R^2=0.91$ ,  $Reff=0.81$ ) periods on daily time scale in the CRB. The HBV was thereafter deployed for prediction of streamflow changes and composition in the CRB using Assessment Report 5 (AR5) based projections. Projected patterns indicated significant changes in flows with up to 26.7% increase that were attributed to up to 6.6 °C increase in the temperature under a high end emission scenario over the basin. Whereas a loss in contribution of snow was seen, a simultaneous increase of up to 28% in the contribution of glacier melt with significant density increase is projected for the flow regime under the high end emission scenario. Moreover, the significant increase in glacier melt was found in phase with residence of high temperatures forced with the emission scenarios in the CRB over the projected periods.

**Contribution/Originality:** This study assesses frequency shifts in high and low magnitude temperature and discharge data in the projections to address attributions to changes seen in the future periods.

### 1. INTRODUCTION

They feed many rivers; amongst them are seven of Asia's greatest rivers - Brahmaputra, Ganges, Huang Ho, Indus, Mekong, Salween and Yangtze. These rivers directly affect the lives of two and a half billion people living in the Hindukush-Himalayan basins. Hindukush-Himalayan snow and glacial melt supply up to 50 % of the average flow of the major rivers in the region. For example, in the 'shoulder seasons', before and after precipitation from the summer monsoon, 70 percent of the flow of the Ganges, Indus, Tarim, and Kabul rivers depend on Hindu Kush and Himalayan melt water. In Western China, glacial melt provides principal water source in dry season for 25 % of the population [1].

The complexity and mutual inter-dependency of mountain environmental and socio-economic systems pose significant problems for climate impact studies [2]. Climate change is expected to contribute to increased variability of river runoff due to changes in timing and intensity of precipitation, as well as melting of snow [3]. In

literature, runoff is widely found to increase as the snow melts which contributes significantly to the flow regime of basins in the Hindukush Ranges [4].

In perspective of recent climate change, future water resources are becoming more significant for planners to allocate and utilize the water ([5]; [6]). General circulation models (GCMs) have been observed as the best tool for projections of future scenarios in context of climate change [7]. Generally, the impact of climate change on hydrological regime is evaluated by using outputs of GCMs as an input to a calibrated hydrologic model ([8]; [9]; [10]; [11]).

In present study, Hydrologiska Byrans Vattenbalansavdelning Light model (HBV) is engaged to predict streamflow of Chitral River Basin (CRB) under climate change scenarios proposed by Intergovernmental Panel on Climate Change (IPCC) based on Fifth Assessment Report (AR5). Sagar, et al. [12] acquired projections from the PRECIS-RCM and used them as input to the HBV for prediction of future streamflow of Karnali River Basin, Nepal for the time period between 2030 and 2060 under A1B of Special Report on Emission Scenarios (SRES). Also in not too distant past, Todorovic and Plavsic [13] used the outputs from five GCM-RCM chains, presented by Langsholt, et al. [14] as input in the HBV model to predict future streamflow of Kolubara River catchment, Serbia.

Since flow forecasting with respect to the climate change could provide significant benefits for the management of national planning strategies, the current study analyzes baseline conditions and uses them to project future variations in the hydro-meteorological regime of the CRB. This study further assesses frequency shifts in high and low magnitude temperature and discharge data in the projections to address attributions to changes seen in the future periods.

## 2. MATERIALS AND METHODS

### 2.1. Study Area

The study area was targeted over the CRB located at the north-western realms of Pakistan with geographical coordinates ranging between 71–74° East Longitude and 36–37° North Latitude Figure 1. It bordered Afghanistan to the west and hosted a significant drainage system in the Hindukush Region. The CRB drained in to the Kabul River which was a sub-catchment of the greater Indus River Basin. The flow of the CRB comprised of snowmelt water and small to large scale glaciers located downstream [15]. Our calculated surface area of the CRB was 12400 Km<sup>2</sup> at the pour point. It held major portion of the glacier cover of the Hindukush range and constituted nearly 10–13% of its area as glacier. Of our calculated magnitudes of areas, vegetation zone covered approximately 10751 Km<sup>2</sup>, barren land covered approximately 423 Km<sup>2</sup> and glaciated zone covered approximately 1226 Km<sup>2</sup> of the basin. Elevation of the basin ranged from 1473 m ASL (Above Sea Level) to 7603 m ASL. For the period of our analysis, average temperature was calculated as 16.3°C, average precipitation as 469 mm/year and average flow as 108067 m<sup>3</sup>/year over the basin. The CRB has remained prone to climate related hazards like temperature triggered glacier lake outburst floods which contributed significantly to the flow regimes especially in summer season over the basin (see e.g., Burhan, et al. [16]).

### 2.2. Data Description

The hydrological data for the time period 1994–2012 was obtained from Surface water hydrology project (SWHP) of Water and Power Development Authority (WAPDA, Pakistan), while the meteorological data was provided by Pakistan Meteorological Department (PMD) for the same time period. Evapotranspiration data was derived from Irmak, et al. [17] using incoming solar radiation and mean temperature data provided by the PMD. Chitral station was located at 35° 51' 48" latitude and 71° 47' 15" longitude, with an elevation of 1500 m ASL. Simulated and projected ensemble climate data of four statistically downscaled GCMs forced by RCP 2.6, 4.5, 6.0, and 8.5 were used for projection analysis Table 1.

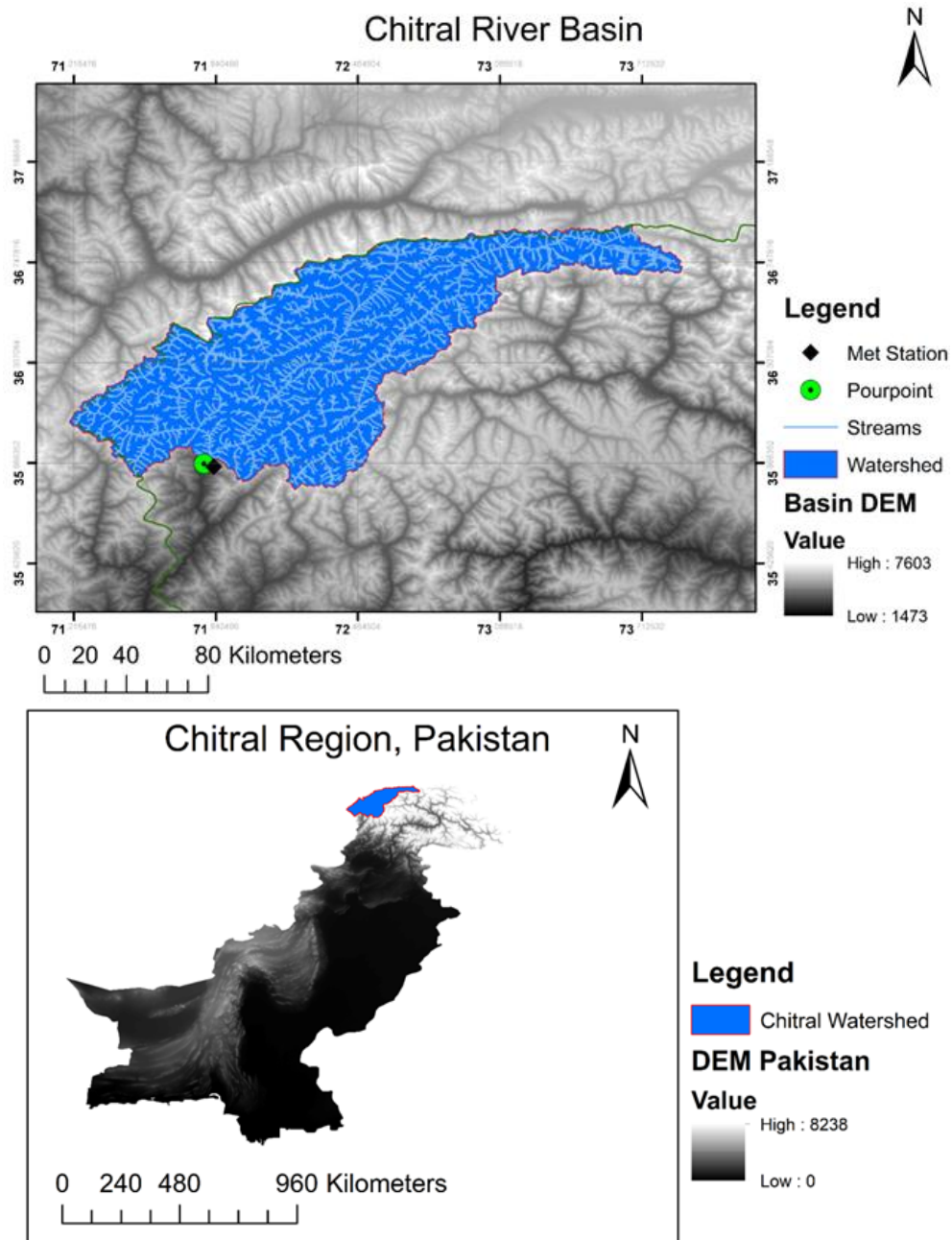


Figure-1. Location of study area with delineated watershed and topography of the CRB. Location of meteorological station (PMD) and flow gauging station (SWHP) is pointed out over the basin.

For ease of use in successive analysis, a nomenclature was defined for control period with baseline representing 1950–2005, and each of the 30 years projected periods with P1 representing 2010–2039, P2 representing 2040–2069 and P3 representing 2070–2099 for all the RCPs used in the study.

Table-1. Description of the GCMs used in this study.

Climate models (GCMs)	Horizontal Resolution	Simulation Period	Institute	Statistically Downscaled	Temporal Frequency	Station
Gfdl-Esm2m	50Km	1950–2099	GFDL	Yes	Daily	Chitral
Ipsl-Cm5a-Lr	50Km	1950–2099	IPSL	Yes	Daily	Chitral
Miroc-Esm-Chem	50Km	1950–2099	MIROC	Yes	Daily	Chitral
Noresm1-M	50Km	1950–2099	Earth Clim	Yes	Daily	Chitral

### 2.3. HBV Modules Engaged in the Study

The HBV model was developed at the Swedish Meteorological and Hydrological Institute (SMHI) to forecast inflow to hydropower stations, but over the years it has been used for various applications due to its development, such as, for hydrological impacts of projected climate change, and flood forecasting [19].

The HBV could be classified as a semi-distributed conceptual model (rainfall-runoff model) of catchment hydrology. The model was based on conceptual representations of physical processes of water flow lumped over entire catchment area. It could reproduce historical daily discharge with an acceptable accuracy [20]. As seen in Figure 2, it depended on daily rainfall, air temperature, long-term monthly mean potential evapotranspiration, streamflow, elevation and vegetation zones, which was also considered as its advantage over other physically based hydrological models to simulate the daily streamflow at a basin outlet ([21]; [22]).

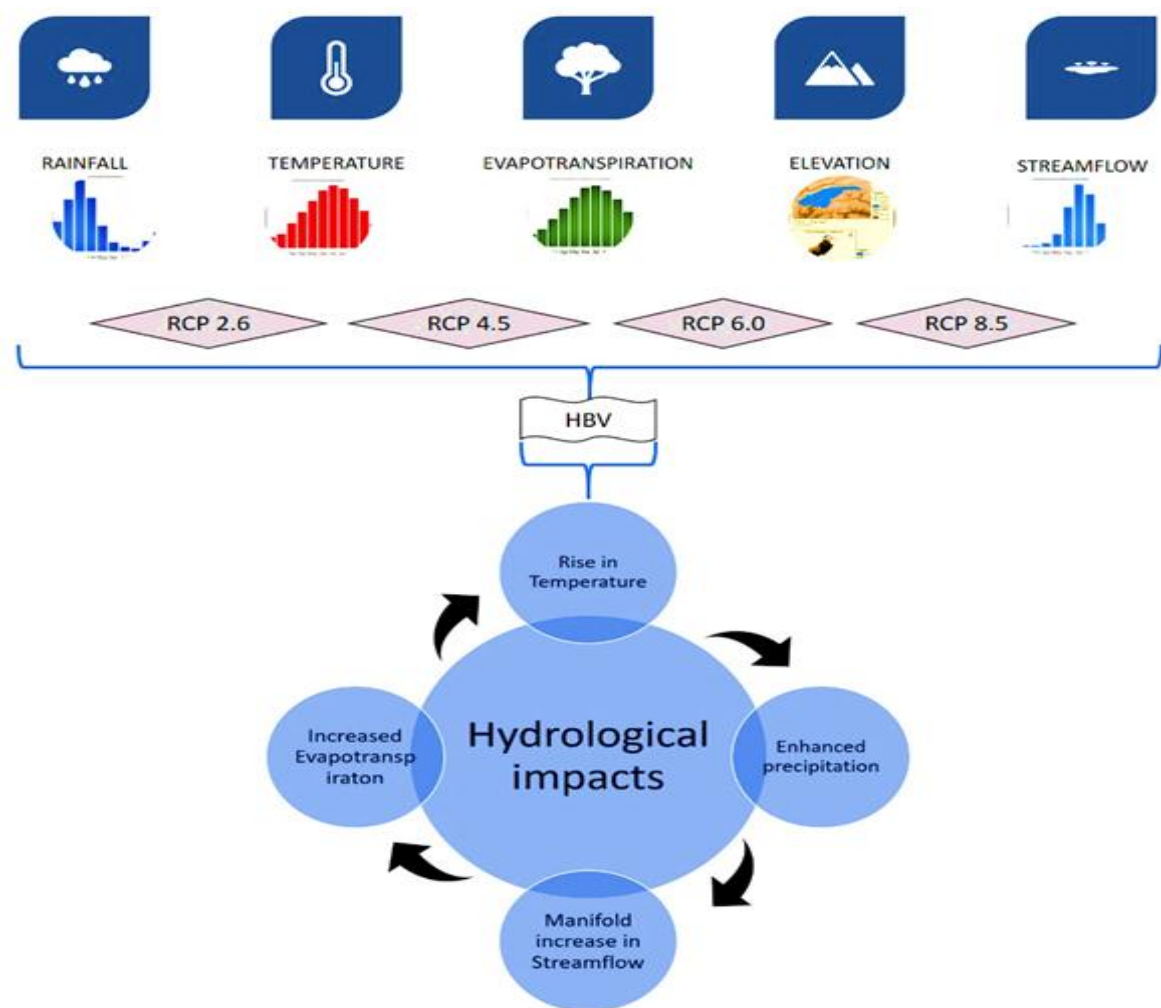


**Figure-2.** Dependency of the HBV on daily rainfall, air temperature, long-term monthly mean potential evapotranspiration, digital elevation model and discharge to simulate daily streamflow at the basin outlet.

Simulated precipitation was termed as snow when temperature went below threshold temperature  $TT$  [ $^{\circ}C$ ] or as liquid rain if temperature went above the  $TT$ . All precipitation simulated as snow was multiplied by a snowfall correction factor, SFCF [-]. A degree-day method was used to calculate snowmelt as seen in Equation 1.

$$melt = CFMAX(T(t) - TT) \quad (1)$$

Meltwater and rainfall was reserved in a snowpack until it exceeded a certain fraction,  $CWH [-]$ , of the water equivalent of the snow. According to Equation 2 refreezing of liquid water occurred by scaling *melt* with refreezing coefficient  $CFR [-]$  within the snowpack.

$$refreezing = CFR CFMAX(TT - T(t)) \quad (2)$$

Depending on relation between water content of soil box  $SM [mm]$  and its largest value  $FC [mm]$ , snowmelt and rainfall were separated into water filling the soil box and groundwater recharge Equation 3.

$$\frac{recharge}{P(t)} = \left(\frac{SM(t)}{FC}\right)^{BETA} \quad (3)$$

Where  $P$  aliased time attributed precipitation and  $BETA$  determined relative contribution to runoff from rain or snowmelt.

According to Equation 4 actual evaporation from soil box equalled potential evaporation if  $\frac{SM}{FC}$  remained greater than soil moisture value above which actual evapotranspiration reached potential evapotranspiration  $LP [-]$ , while a linear reduction was used when  $\frac{SM}{FC}$  remained below the  $LP$ .

$$E_{act} = E_{pot} \min\left(\frac{SM(t)}{FC \cdot LP}, 1\right) \quad (4)$$

Groundwater recharge was added to upper groundwater box  $SUZ [mm]$ . Maximum percolation rate from the  $SUZ$  to the lower groundwater box  $SLZ [mm]$  was described by PERC  $[mm/day]$ . In Equation 5 runoff that was generated from the groundwater boxes was computed as the sum of two or three linear outflow equations, and it depended on whether  $SUZ$  was above a threshold value  $UZL [mm]$ .

$$Q_{GW}(t) = K_2 SLZ + K_1 SUZ + K_0 \max(SUZ - UZL, 0) \quad (5)$$

Where  $Q_{GW}$  was time attributed groundwater recharge, and  $K_0$ ,  $K_1$  and  $K_2$  were storage (or recession) coefficients of respective groundwater boxes.

To simulate daily discharge values  $Q_{sim} [mm/day]$  the runoff was finally transformed by a triangular weighting function defined by the parameter MAXBAS according to Equation 6.

$$Q_{sim}(t) = \sum_{i=1}^{MAXBAS} c(i) Q_{GW}(t-i+1) \quad (6)$$

$$\text{Where } c(i) = \int_{i-1}^i \frac{2}{MAXBAS} - \left| u - \frac{MAXBAS}{2} \right| \frac{4}{MAXBAS^2} du$$

with  $u$  being a time function.

Since multiple elevation zones were used in this study, variations in precipitation and temperature with elevation were calculated using two parameters  $PCALT$  (%/100 m) and  $TCALT$  (°C/100 m) given in Equation 7 and 8.

$$P(h) = P_0 \left( 1 + \frac{PCALT(h-h_0)}{10000} \right) \quad (7)$$

$$T(h) = \frac{T_0 - TCALT(h-h_0)}{100} \quad (8)$$

Where  $P(h)$  and  $T(h)$  were varied precipitation and temperature values respectively at height  $h$  with respect to a reference height  $h_0$ .

The long-term mean of potential evaporation,  $E_{pot,M}$  for a certain day of the year was corrected to its value at day  $t$ ,  $E_{pot}(t)$ , by using deviations of temperature,  $T(t)$ , from its long-term mean,  $T_M$ , and a correction factor,  $C_{ET}$  [°C<sup>-1</sup>] according to Equation 9.

$$E_{pot}(t) = (1 + C_{ET}(T(t) - T_M)) E_{pot,M} \quad (9)$$

$$\text{But } 0 \leq E_{pot}(t) \leq 2E_{pot,M}$$

#### 2.4. Model and Catchment Settings

In current version of the HBV, snow melt routine along with glacier ice melt and accumulation were deployed. Moreover, to present effect of different expositions on snow and ice melts, a spatial discretization in aspect classes including South, North and East–West–Horizontal was introduced. Glacier ice melt was simulated using similar degree-day method as of snow, however with the degree-day factor being increased for the melting of ice as compared to snow due to its lower albedo. Since the CRB constituted of 10–13% glaciers whose melt is a major contributor to its stream flow, the selected model was found viable to be applied over the glaciated watershed.

Considering first year as warm up period, fourteen years were selected for calibration of the HBV, starting from 1994–2007, while 2008–2012 were used for the validation/verification of the model. The CRB watershed is delineated using Shuttle Radar Topography Mission (SRTM) 90m Digital Elevation Model (DEM). Sentinel-2A/2B earth observation satellite data was used for configuration of vegetation, barren and glaciation zones for seven elevation levels (1910–7165m) using Normalized Difference Vegetation Index (NDVI) and Normalized

Difference Snow Index (NDSI) (<https://eos.com/index-stack/>) Figure 3. Optimum calibration values for the HBV parameters in the vegetation, the barren and the glaciation zones are presented in Appendix 1.

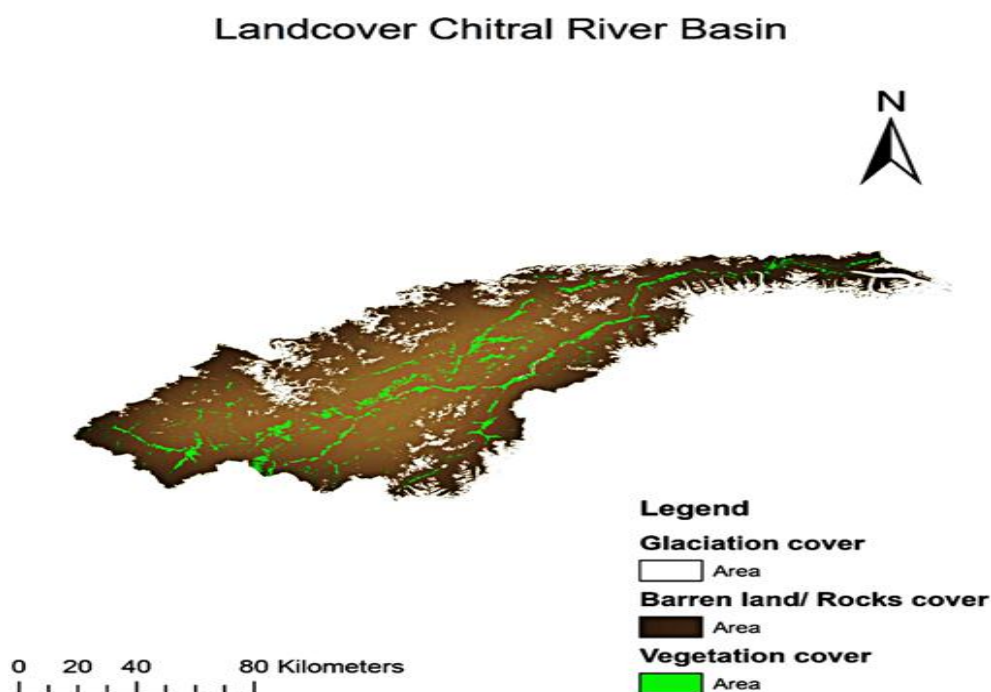


**Figure-3.** Fractions of landcover zones identified using NDVI and NDSI over the CRB and deployed in the HBV.

### 2.5. Construction of Probability Density Functions

Probability density functions were modelled owing to their advanced type of statistical measuring function with applications in climate change and its diagnostics (see e.g. Burhan [23]). The density functions provided to correlate random occurrences to their probability. Since probability density function helped calculate cumulative distributions, we engaged it for calculation of flow and temperature densities in order to rationalize attributions of changing patterns over the projections. Thereafter, based on the fitted distribution, frequencies, relative frequencies, and densities for the changes in projections were computed.

## 3. RESULTS

### 3.1. Calibration and Validation Results

Calibration and validation output over the catchment area is shown in Figure 4. The coefficient of efficiency is determined by using statistical approach of Nash–Sutcliffe model efficiency coefficient (NSE) which is used to assess the predictive power of hydrological models. An  $R_{\text{eff}}$  value close to 1 indicates a virtually perfect fit. The HBV model performed fairly well both during calibration ( $R^2=0.91$ ,  $R_{\text{eff}}=0.91$ , PBIAS=3.7%) and validation ( $R^2=0.82$ ,  $R_{\text{eff}}=0.81$ , PBIAS=-2.0%) periods on daily time scale in the CRB.

### 3.2. Analysis of Ensemble Projected Flow and its Attributions

In the P1, it is seen that overall discharge projections for ensemble of GCMs show significant decrease under all the emission scenarios with highest decrease of 7.5% under the RCP8.5 emissions scenario. As is seen in Table 2, in the P2, the overall flow projections decrease under the RCP2.6 (0.5% decrease), however, under all the remaining emission scenarios it is seen to increase by up to 4.5% under the RCP8.5 emission scenario. Similar patterns of increase and decrease are seen in the P3 with a decreasing flow projection (3.4%) under the RCP2.6 emission

scenario, whilst an increasing flow is projected under all the remaining emission scenarios with up to 26.7% increase under the RCP8.5 emission scenario.

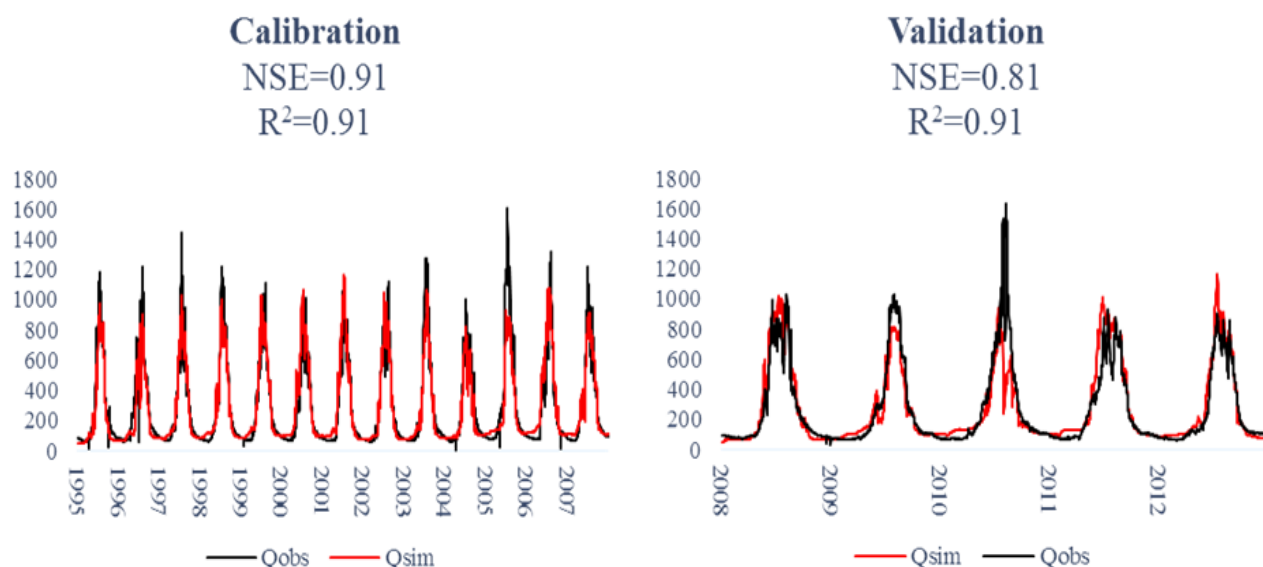


Figure-4. Emulation of calibrated and validated flows of the CRB with NSE and  $R^2$  values representing high efficiency in model predictions.

In sense of projected periods, the results also show that with the exception of RCP2.6, the remaining emission scenarios project a decrease of flow in the P1 with a successive robust increase in the P2 and the P3 indicating prominence of increase over decrease in overall projected flows of the basin. Projected patterns of increasing flows in the basin found under this study are in line with findings of LEAD [4].

In terms of precipitation projections, majority of the designated periods as well as the emission scenarios display an overall decrease which is exceptionally high under the RCP8.5 emission scenario. In Table 2, it is depicted that only RCP2.6, owing to its moderate rate of emissions and modest amount of solar radiation intensity displays an up to a percent increase in the P1 which remains insignificant when compared with large deficient changes in the other periods and the scenarios. In the P1, both RCPs 4.5 and 8.5 show outstanding negative changes in precipitation with up to 4.7% decrease under the RCP 8.5 emission scenario. The P2 further decreases projected precipitation with up to 9.1% decrease under the RCP8.5 emission scenario. The change is highest in the P3 where all the emission scenarios project decrease ranging from 1.3 to 9.9% deficient precipitation over the basin. It is also interesting to see that in transition from the P1 to P3, deficiency in precipitation increases and this trend pattern remains consistent for all the emission scenarios. In defense of analyzed projected direction of change in precipitation, there is evidence that in the 21st century, precipitation has been stated to decrease by up to 50% across Kabul River Basin of which the CRB is a sub-basin [24].

The four GCMs ensemble suggests an overall increase in projected temperature over the CRB, under all the RCPs in all the time periods, as shown in Table 2. The minimum value of temperature increase is 1.6 °C falling under the RCP4.5 in the P1, whereas the maximum value of temperature increase is 6.6 °C falling under the RCP8.5 in the P3. As is anticipated, the temperature changes are seen to progress in successive periods under all the RCPs with highest progression change seen in the RCP8.5 emission scenario. In fact, range in progression from minimum temperature change to maximum temperature change attains a value of 4.2 °C under the RCP8.5 emission scenario in contrast to a modest value of 0.5 °C under the RCP2.6 emission scenario. Overall consensus of all the four models suggests an increase in temperature of the river basin throughout the 21st century, with the change being more prominent and strong towards end of the century.

The ensemble projections of evapotranspiration for the three time periods reveal an overall increase over the basin under all the emission scenarios. It is provided in Table 2, that, in the P1, the percent increase of the

evapotranspiration ranges between 4.4 to 5.9 under the RCP2.6 emission scenario in contrast to that in the P3 which ranges between 4.9 to 16.8 under the RCP8.5 emission scenario. The inter-scenario ranges for change in evapotranspiration varies from 0.9% in the P1, to 6.6% in the P2, and further up to 10.9% in the P3 which indicates time borne progression in the projected evapotranspiration. The high end scenario projections for evapotranspiration generally attributes to loss in soil moisture which eventually affects flow regimes and runoffs over the basins. However since magnitude of projected flow outstands significantly from the magnitude of the projected increase in evapotranspiration, it hardly effects the flow regime to any significant level of interest.

**Table-2.** Changes in projected flows (%), precipitation (%), temperature (°C), and evapotranspiration (%). Statistically significant changes are presented by \*= p-value<0.05, \*\*= p-value <0.01, and \*\*\*= p-value <0.001.

Projected changes in flows (%)					
	Time Period	RCP 2.6	RCP 4.5	RCP 6.0	RCP 8.5
P1	2010-2039	*-3.4	** -5.6	-1.9	***-7.5
P2	2040-2069	-0.5	0.4	0.9	4.5
P3	2070-2099	** -3.8	*5.1	*6.9	***26.7
Projected changes in precipitation (%)					
P1	2010-2039	1.0	***-3.4	-0.4	-4.7
P2	2040-2069	0.2	***-5.1	-0.8	-9.4
P3	2070-2099	-1.3	***-5.7	*-7.6	-9.9
Projected changes in temperature (°C)					
P1	2010-2039	***1.8	***1.6	***1.6	***2.0
P2	2040-2069	***2.0	***3.0	***2.7	***4.2
P3	2070-2099	***2.3	***3.9	***4.3	***6.6
Projected changes in evapotranspiration (%)					
P1	2010-2039	***4.4	***4.1	***4.0	***4.9
P2	2040-2069	***4.3	***7.7	***6.5	***10.9
P3	2070-2099	***5.9	***10.6	***11.6	***16.8

As is seen from Table 3, both the baseline and projections show the snow component as the major contributor to flow regime of the basin. Simulated streamflow analysis based on ingested GCMs data unveils that average percentage composition of snow and glacier melt to the streamflow of the CRB is about 98.7%, and 0.8% respectively for the baseline period. It is interesting to find that with progression of the periods, contribution of snow regime declines from 98.7% in the baseline, to 95.5% in the P1 under the RCP6.0 emission scenario, and further down to 70.4% in the P3 under the RCP8.5 emission scenario over the basin.

**Table-3.** Projected percent changes in contribution of simulated rain, snowmelt, and glacier melt to discharge in the CRB.

	RCP 2.6			RCP 4.5			RCP 6.0			RCP 8.5		
Time Period	Rain	Snow	Glacier									
2010-2039 (P1)	0.2	95.2	4.4	0.2	95.1	4.6	0.2	95.5	4.2	0.2	94.6	5.1
2040-2069 (P2)	0.2	94.8	4.9	0.2	88.6	11.0	0.2	92.2	7.4	0.2	83.5	16.0
2070-2099 (P3)	0.2	94.0	5.6	0.2	87.4	12.2	0.2	83.0	16.5	0.1	70.4	29.1

Whereas a loss in contribution of snow is seen, a simultaneous increase in the contribution of glacier melt is projected which ranges from 0.8% in the baseline, to 29.1% in the P3 under the RCP8.5 emission scenario. However it is also of significance to note that no major changes in contribution of liquid precipitation is seen in the overall projections of the flow under all the emission scenarios over the basin. Ahmad, et al. [15] advocates strong dependency of the CRB flow on snowmelt driven by the temperature, and hence augments our findings of the projected stream flow composition over the basin.

3.3. Assessment of Frequency Distribution of Temperatures and Driven Flows

The probability density functions of temperature regime show majority of decreases in low magnitude bins and corresponding increases in high magnitude bins under all the RCPs except the RCP2.6, as depicted in Figure 5, and similar is endorsed by Burhan and Rasul [25]. The overall changes in the frequency distributions display the RCP4.5 to hold highest frequency changes both in the P2 and the P3 with at least 25 more occurrences of temperature bins ranging from -5.7 to -2.8 °C. This further holds that the mentioned temperature bin is suggested to increase its probability of occurrence from null to more than 86% in the projection periods which may be taken as a major contributor to other attributed changes. Whereas increase in frequency of high magnitude bins of temperature has impacts, simultaneous decreases in frequencies of low magnitude bins of the same also have tendency to maintain moderation in increasing temperatures. It is seen that the temperature bin ranging from -8.9 to -7.7 °C has shown highest decrease by dropping down its probability of occurrence from 72% to nearly 0% in all the projected periods under the RCP8.5 emission scenario.

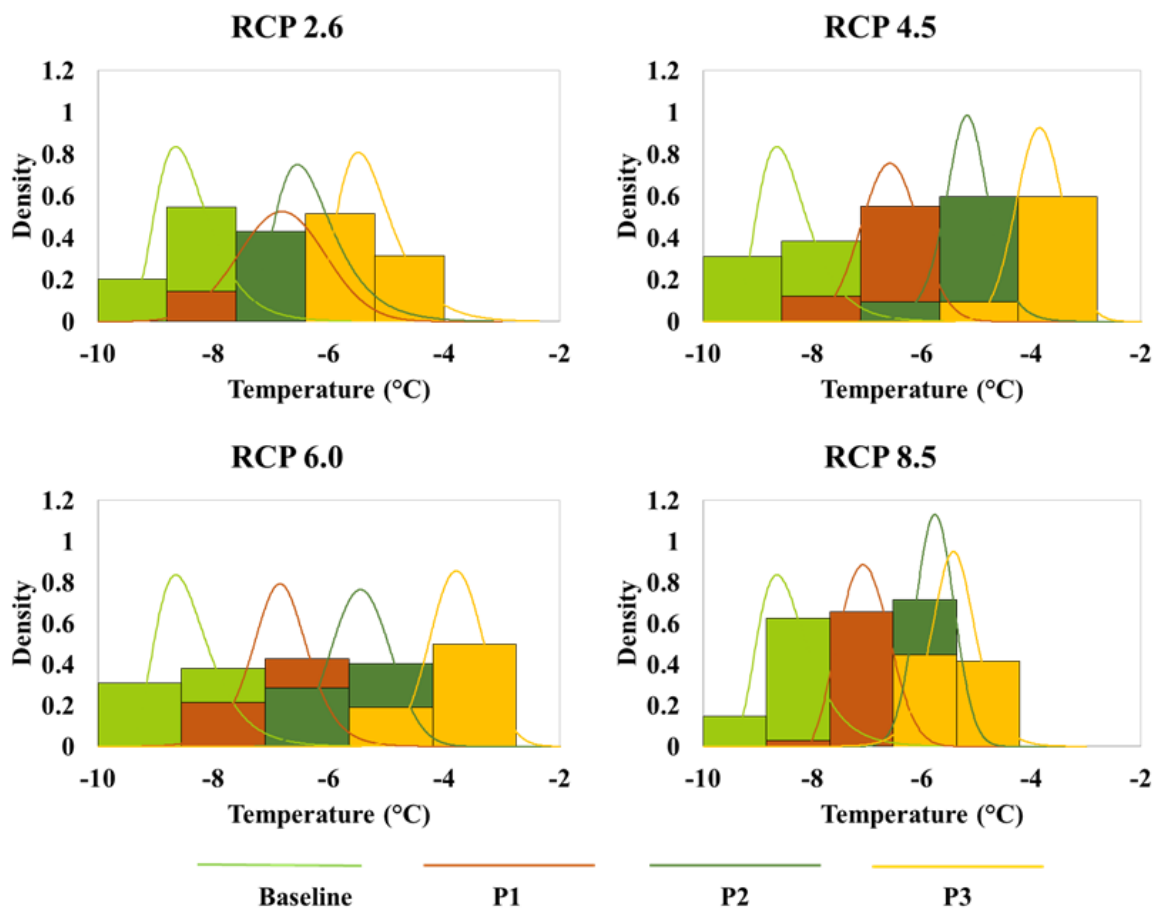
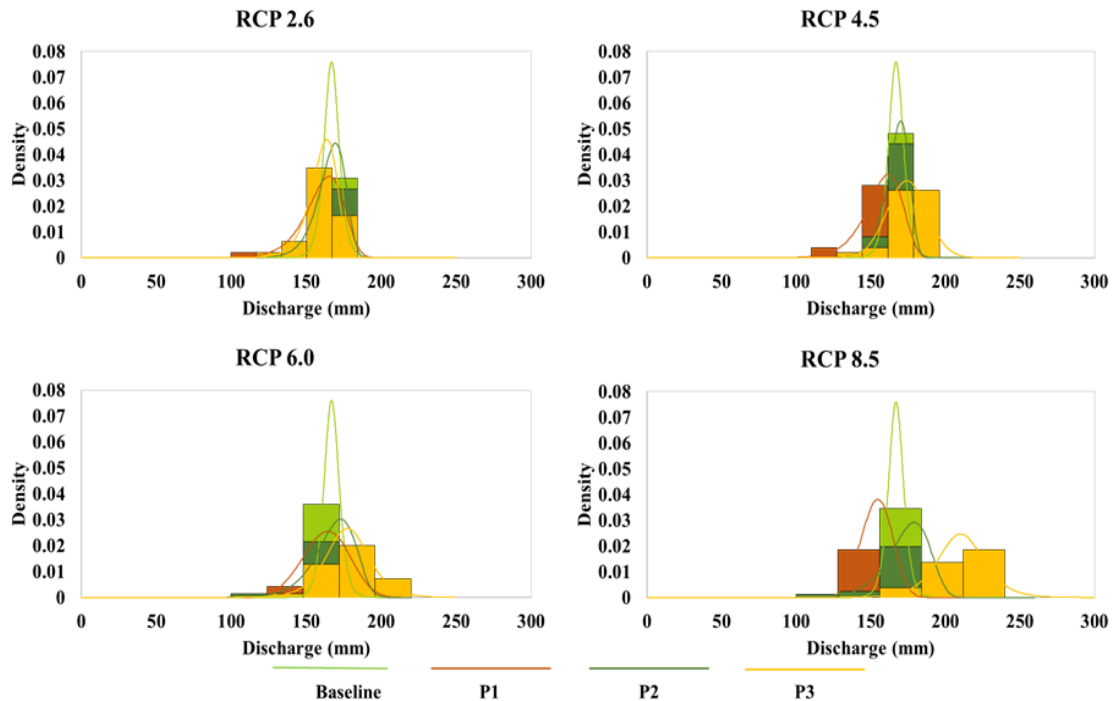


Figure-5. Probability density functions of temperature (°C) for the baseline and projected periods under all examined RCPs. Time borne shifts in temperature extremes can be seen clearly as periods progress from the baseline to the future projections.

As illustrated in Figure 6, in the flow regime, the density functions show significant variations in changing patterns in all the projected periods with highest of them being observed under the RCP8.5 emission scenario. Of all the changes seen, the stream flow of bin ranging from 212 mm to 240 mm show highest frequency change with 15 more occurrences in the P3 under the RCP8.5 emission scenario. Resultantly the probability of occurrence of the 212 mm to 240 mm bin range is seen to increase from being null in the baseline to become 52% in the P3 which projects a significant addition of high magnitude flows in the future periods. Shifts are seen to transit from low magnitude flows to high magnitude flows in the projections and are most prominent in 156 mm to 184 mm bin in the P3 with 25 less occurrences under the RCP8.5 emission scenario. The baseline flow of the 156 mm to 184 mm

bin is seen to recur with probability of 96%, however owing to the mentioned frequency decrease, the probability of occurrence drops down to nearly 10% in the P3. This indicates that the frequency shift in temperature from low magnitude bins to high magnitude bins is in phase with the flow frequency shift from the low magnitude bins to high ones. It further provides an evidence for increase in frequency of high magnitude flows being an effect of temperature borne melt which contributes in major portion of the projected flow.



**Figure-6.** Probability density functions of discharge (mm) for the baseline and projected periods under all examined RCPs. Time borne shifts in flow regimes can be seen clearly as periods progress from the baseline to the future projections.

#### 4. CONCLUSIONS

Projected changes in the stream flow of the CRB are analyzed using the high resolution statistically downscaled GCMs output as input to the hydrological model HBV under the four AR5 based RCP emission scenarios. The HBV performed fairly well both during calibration and validation periods on daily time scale over the CRB. Projected patterns indicate significant increase in flows over the basin. Overall consensus of GCMs ensemble suggests an increase in temperature of the river basin throughout the 21<sup>st</sup> century, with the change being more prominent and strong towards the end of the century. Analyzed projected direction of change in precipitation is negative which indicates decrease in precipitation through the 21<sup>st</sup> century over the basin. However since magnitude of projected flow outstands significantly from the magnitude of the projected decrease in liquid precipitation, it hardly effects the flow regime to any significant level of interest. Whereas a loss in contribution of snow is seen, a simultaneous increase in the contribution of glacier melt is projected in future flows. The frequency shift in temperature from low magnitude bins to high magnitude bins is in phase with the flow frequency shift from the low magnitude bins to high ones. It therefore provides rationale for increase in frequency of high magnitude flows being an effect of temperature borne melt which contributes to a major share of the projected flow.

**Funding:** The authors acknowledge motivation for quality research supported by joint research projects No. PSF/NSFC/Earth-/C-PMD (08) and No. PSF/NSFC/Earth-/C-PMD(10).

**Competing Interests:** The authors declare that they have no competing interests.

**Acknowledgement:** All authors contributed equally to the conception and design of the study.

## REFERENCES

- [1] X. Jianchu, A. Shrestha, R. Vaidya, M. Eriksson, and K. Hewitt, *The melting Himalayas. Regional challenges and local impacts of climate change on Mountain ecosystems and livelihoods*. Kathmandu: ICIMOD Technical Paper, 2007.
- [2] H. F. Diaz, M. Beniston, and R. S. Bradley, "Climatic change at high elevation sites," ed Netherlands: Springer, 1997, pp. 1-298.
- [3] X. Fang and J. W. Pomeroy, "Snowmelt runoff sensitivity analysis to drought on the Canadian prairies," *Hydrological Processes: An International Journal*, vol. 21, pp. 2594-2609, 2007. Available at: <https://doi.org/10.1002/hyp.6796>.
- [4] P. LEAD, *Impact of the 21st century climate change on surface water availability of the Transboundary Kabul River Basin: LEAD Pakistan*, 2018.
- [5] N. Arnell, "Climate-change impacts on river flows in Britain: the UKCIPO2 scenarios," *Water and Environment Journal*, vol. 18, pp. 112-117, 2004. Available at: <https://doi.org/10.1111/j.1747-6593.2004.tb00507.x>.
- [6] Y. Shen, T. Oki, N. Utsumi, S. Kanae, and N. Hanasaki, "Projection of future world water resources under SRES scenarios: Water withdrawal / projection of future global water resources according to SRES scenarios: Water withdrawal," *Hydrological Sciences Journal*, vol. 53, pp. 11-33, 2008.
- [7] C.-y. Xu, "Climate change and hydrologic models: A review of existing gaps and recent research developments," *Water Resources Management*, vol. 13, pp. 369-382, 1999.
- [8] F. H. S. Chiew, I. P. Prosser, and D. A. Post, "On climate variability and climate change and impact on water resources," presented at the 19th International Congress on Modelling and Simulation, Perth, Australia, 12-16 December, 2011.
- [9] A. Kay, H. Davies, V. Bell, and R. Jones, "Comparison of uncertainty sources for climate change impacts: Flood frequency in England," *Climatic Change*, vol. 92, pp. 41-63, 2009. Available at: <https://doi.org/10.1007/s10584-008-9471-4>.
- [10] J. Teng, F. Chiew, J. Vaze, S. Marvanek, and D. Kirono, "Estimation of climate change impact on mean annual runoff across continental Australia using Budyko and Fu equations and hydrological models," *Journal of Hydrometeorology*, vol. 13, pp. 1094-1106, 2012. Available at: <https://doi.org/10.1175/jhm-d-11-097.1>.
- [11] R. Wilby and I. Harris, "A framework for assessing uncertainties in climate change impacts: Low flow scenarios for the River Thames," *Water Resources Research*, vol. 42, p. W02419, 2006. Available at: <https://doi.org/10.1029/2005wr004065>.
- [12] S. Sagar, D. Roberts, B. Bala, and L. Lyburner, "Extracting the intertidal extent and topography of the Australian coastline from a 28 year time series of Landsat observations," *Remote Sensing of Environment*, vol. 195, pp. 153-169, 2017. Available at: <https://doi.org/10.1016/j.rse.2017.04.009>.
- [13] A. Todorovic and J. Plavsic, "The role of conceptual hydrologic model calibration in climate change impact on water resources assessment," *Journal of Water and Climate Change*, vol. 7, pp. 16-28, 2015.
- [14] E. Langsholt, D. Lawrence, W. K. Wong, M. Andjelic, M. Ivkovic, and M. Vujadinovic, *Effects of climate change in the Kolubara and Toplica catchments*. Serbia: Norwegian Water Resources and Energy Directorate Editor, 2013.
- [15] S. Ahmad, M. Israr, S. Liu, H. Hayat, J. Gul, S. Wajid, M. Ashraf, S. U. Baig, and A. A. Tahir, *Spatio-temporal trends in snow extent and their linkage to hydro-climatological and topographical factors in the Chitral River Basin*. Hindukush, Pakistan: Geocarto International, 2018.
- [16] A. Burhan, M. K. Abuzar, R. A. Shafiq, R. Kiran, R. Manzoor, and S. Kubra, "Diagnostic study of heavy downpour in 2015 flash floods over Chitral Area, Northern Pakistan," *Pakistan Journal of Meteorology*, vol. 12, pp. 79-93, 2016.
- [17] S. Irmak, A. Irmak, R. Allen, and J. Jones, "Solar and net radiation-based equations to estimate reference evapotranspiration in humid climates," *Journal of Irrigation and Drainage Engineering*, vol. 129, pp. 336-347, 2003. Available at: [https://doi.org/10.1061/\(asce\)0733-9437\(2003\)129:5\(336\)](https://doi.org/10.1061/(asce)0733-9437(2003)129:5(336)).

- [18] S. Buda, H. Jinlong, G. Marco, J. Dongnan, T. Hui, J. Tong, and Z. Chengyi, "Statistical downscaling of CMIP5 multi-model ensemble for projected changes of climate in the Indus River Basin," *Atmospheric Research*, vol. 178-179, pp. 138-149, 2016. Available at: <https://doi.org/10.1016/j.atmosres.2016.03.023>.
- [19] D. Lawrence, I. Haddeland, and E. Langsholt, "Calibration of HBV hydrological models using PEST parameter estimation. Retrieved from: [http://publikasjoner.nve.no/report/2009/report2009\\_01.pdf](http://publikasjoner.nve.no/report/2009/report2009_01.pdf)," 2009.
- [20] E. Abebe and A. Kebede, "Assessment of climate change impacts on the water resources of megech river catchment, Abbay Basin, Ethiopia," *Open Journal of Modern Hydrology*, vol. 7, pp. 141-152, 2017. Available at: <https://doi.org/10.4236/ojmh.2017.72008>.
- [21] H. I. J. Al-Safi and P. R. Sarukkalgige, "Assessment of future climate change impacts on hydrological behavior of Richmond River Catchment," *Water Science and Engineering*, vol. 10, pp. 197-208, 2017. Available at: <https://doi.org/10.1016/j.wse.2017.05.004>.
- [22] K. Vormoor, O. Rössler, G. Bürger, A. Bronstert, and R. Weingartner, "When timing matters-considering changing temporal structures in runoff response surfaces," *Climatic Change*, vol. 142, pp. 213-226, 2017. Available at: <https://doi.org/10.1007/s10584-017-1940-1>.
- [23] A. Burhan, "An analysis of climate change in Pakistan," ed Mauritius: Scholar's Press, 2018, pp. 1-126.
- [24] S. A. A. Bokhari, B. Ahmad, J. Ali, S. Ahmad, H. Mushtaq, and G. Rasul, "Future climate change projections of the Kabul River Basin using a multi-model ensemble of high-resolution statistically downscaled data," *Earth Systems and Environment*, vol. 2, pp. 477-497, 2018. Available at: <https://doi.org/10.1007/s41748-018-0061-y>.
- [25] A. Burhan and G. Rasul, "Statistically downscaled projections of CORDEX South Asia using quantile mapping approach over Pakistan region," *International Journal of Global Warming*, vol. 16, pp. 435-460, 2018.

## APPENDIX

**Appendix-1. Optimum calibrated values for the vegetation, the barren and the glaciation zones of the HBV.**

HBV Parameters		Vegetation zone		Barren zone		Glaciation zone	
KSI	0.250100806	TT	-4.12951415	TT	-4.685199792	TT	-3.527571292
Kgmin	0.017597511	CFMAX	30.88450624	CFMAX	15.90643211	CFMAX	59.60253764
dKG	0.168364443	SP	0.20240973	SP	0.022618238	SP	0.151747514
AG	7.66E-05	SFCF	617.4145185	SFCF	180.8286314	SFCF	454.0538147
PERC	0.00092443	CFR	0.05	CFR	0.05	CFR	0.05
UZL	99.98775923	CWH	0.999850481	CWH	0.21741848	CWH	0.328470837
K0	0.499920062	CFGlacier	4.347784177	CFGlacier	7.914945804	CFGlacier	8.289640226
K1	0.199942682	CFSlope	6.87045674	CFSlope	2.853130089	CFSlope	6.964866733
K2	0.001691414	FC	522.2536635	FC	699.7224643	FC	418.2681649
MAXBAS	2.204186293	LP	0.012485499	LP	0.002337956	LP	0.010317167
Cet	0	BETA	6.773193678	BETA	1.00349888	BETA	7.720007865
PCALT	10						
TCALT	0.6						
Pelev	1497.8						
Telev	1497.8						

*Views and opinions expressed in this article are the views and opinions of the author(s), International Journal of Climate Research shall not be responsible or answerable for any loss, damage or liability etc. caused in relation to/arising out of the use of the content.*